Chapter 5

Quadrilateral Shell Elements.

Flat quadrilateral shell elements have use limitations even in linear analysis, since a mesh that consists of strictly flat elements may be impossibly to construct over a doubly-curved shell surface. For large deflection nonlinear analysis this deficiency becomes more pronounced. Even if the initial mesh satisfies the flat element restriction, the deformations can become so large that warping of the elements can be significant. Finding ways of handling warped element geometries is thus of fundamental importance for quadrilateral shell elements.

The current research initially set out to develop a non-flat quadrilateral element that was able to satisfy self-equilibrium in a warped configuration. This proved to be difficult. Finding a basic stiffness $\mathbf{K}_b = \frac{1}{A}\mathbf{L}\mathbf{C}\mathbf{L}^T$ that maintained self equilibrium was especially troublesome. To achieve this goal one must have the lumped node forces from a constant stress state $\mathbf{f} = \mathbf{L}\boldsymbol{\sigma}$ to be in self equilibrium. Two questions arise at this point: What is a constant stress state for a warped shell element? Is a constant stress state for a warped surface an equilibrium state for arbitrary element shapes? These are key questions that remain to be answered in order to develop satisfactory FF and ANDES elements for such element geometries. It follows that those formulations have to be further extended for developing warped shell elements. The construction of the basic stiffness matrix needs special attention because the Individual Element Test is not clearly defined for curved or warped element geometries.

Restoring equilibrium in the warped element geometry can be done *a posteriori* for elements developed with reference to the flat projected "footprint" by using a projector matrix. This is the approach that has been chosen for the current quadrilateral element. It allows independent development of the membrane and bending components since these two stiffness contributions decouple, which greatly simplifies the development of the element. Both linear and nonlinear projectors have been developed for the quadrilateral element. Both versions give identical results for linear static problems, but the linear projector is recommended for linear finite element codes because its formulation is much simpler than that of the nonlinear projector.

5.1 Geometric definitions for a quadrilateral element.

This section describes geometric relationships for a quadrilateral element. The development covers both warped geometry and the flat "best fit" element obtained by setting the z coordinate for each node equal to zero. The flat projection relationships are later used for the development of the membrane and bending stiffness of the shell element. The non-flat relationships are needed for the development of the nonlinear projector for quadrilaterals.

A vector $\mathbf{r}$ to a point on a nonflat quadrilateral element can be parametrized with respect to the natural coordinates ξ and η as

$$\mathbf{r}(\xi,\eta) = \left\{ \begin{array}{c} x \\ y \\ z \end{array} \right\} = \left[\begin{array}{ccc} \mathbf{N} & \mathbf{0} & \mathbf{0} \\ \mathbf{0} & \mathbf{N} & \mathbf{0} \\ \mathbf{0} & \mathbf{0} & \mathbf{N} \end{array} \right] \left\{ \begin{array}{c} \mathbf{x} \\ \mathbf{y} \\ \mathbf{z} \end{array} \right\}, \tag{5.1.1}$$

where

$$\mathbf{x} = \left\{ \begin{array}{c} x_1 \\ x_2 \\ x_3 \\ x_4 \end{array} \right\}, \qquad \mathbf{y} = \left\{ \begin{array}{c} y_1 \\ y_2 \\ y_3 \\ y_4 \end{array} \right\}, \qquad \mathbf{z} = \left\{ \begin{array}{c} z_1 \\ z_2 \\ z_3 \\ z_4 \end{array} \right\}, \tag{5.1.2}$$

and x_i, y_i and z_i denote the global coordinates of node i. Row vector $\mathbf{N}$ contains the "usual" bi-linear isoparametric interpolation for a quadrilateral [00]. These functions and their partial derivatives with respect to ξ and η are

$$\begin{aligned} \mathbf{N} &= \frac{1}{4}\left[(1-\xi)(1-\eta) \quad (1+\xi)(1-\eta) \quad (1+\xi)(1+\eta) \quad (1-\xi)(1+\eta) \right], \\ \mathbf{N}_{,\xi} &= \frac{1}{4}\left[-(1-\eta) \quad (1-\eta) \quad (1+\eta) \quad -(1+\eta) \right], \\ \mathbf{N}_{,\eta} &= \frac{1}{4}\left[-(1-\xi) \quad -(1+\xi) \quad (1+\xi) \quad (1-\xi) \right]. \end{aligned} \tag{5.1.3}$$

Using these geometric relations the variation of the position vector $\mathbf{r}$ can be written as

$$\left\{ \begin{array}{c} dx \\ dy \\ dz \end{array} \right\} = \left\{ \begin{array}{c} \frac{\partial x}{\partial \xi} d\xi + \frac{\partial x}{\partial \eta} d\eta \\ \frac{\partial y}{\partial \xi} d\xi + \frac{\partial y}{\partial \eta} d\eta \\ \frac{\partial z}{\partial \xi} d\xi + \frac{\partial z}{\partial \eta} d\eta \end{array} \right\} = \left[\begin{array}{cc} \frac{\partial x}{\partial \xi} & \frac{\partial x}{\partial \eta} \\ \frac{\partial y}{\partial \xi} & \frac{\partial y}{\partial \eta} \\ \frac{\partial z}{\partial \xi} & \frac{\partial z}{\partial \eta} \end{array} \right] \left\{ \begin{array}{c} d\xi \\ d\eta \end{array} \right\} \tag{5.1.4}$$

$$= \left[\begin{array}{cc} \mathbf{N}_{,\xi}\mathbf{x} & \mathbf{N}_{,\eta}\mathbf{x} \\ \mathbf{N}_{,\xi}\mathbf{y} & \mathbf{N}_{,\eta}\mathbf{y} \\ \mathbf{N}_{,\xi}\mathbf{z} & \mathbf{N}_{,\eta}\mathbf{z} \end{array} \right] \left\{ \begin{array}{c} d\xi \\ d\eta \end{array} \right\} = \left[\mathbf{g}_\xi \quad \mathbf{g}_\eta \right] \left\{ \begin{array}{c} d\xi \\ d\eta \end{array} \right\}$$

or

$$d\mathbf{r} = \mathbf{J} d\boldsymbol{\xi} \, .$$

The Jacobian $\mathbf{J}$ introduced above is also used for computing partial derivatives with respect to the natural coordinates ξ and η:

$$\begin{aligned}\left\{\begin{array}{c}\frac{\partial(\cdot)}{\partial\xi}\\ \frac{\partial(\cdot)}{\partial\eta}\end{array}\right\} &= \left\{\begin{array}{c}\frac{\partial(\cdot)}{\partial x}\frac{\partial x}{\partial\xi}+\frac{\partial(\cdot)}{\partial y}\frac{\partial y}{\partial\xi}\\ \frac{\partial(\cdot)}{\partial x}\frac{\partial x}{\partial\eta}+\frac{\partial(\cdot)}{\partial y}\frac{\partial y}{\partial\eta}\end{array}\right\} = \left[\begin{array}{cc}\frac{\partial x}{\partial\xi} & \frac{\partial y}{\partial\xi}\\ \frac{\partial x}{\partial\eta} & \frac{\partial y}{\partial\eta}\end{array}\right]\left\{\begin{array}{c}\frac{\partial(\cdot)}{\partial x}\\ \frac{\partial(\cdot)}{\partial y}\end{array}\right\}\\ &= \left[\begin{array}{cc}\mathbf{N}_{,\xi}\mathbf{x} & \mathbf{N}_{,\xi}\mathbf{y}\\ \mathbf{N}_{,\eta}\mathbf{x} & \mathbf{N}_{,\eta}\mathbf{y}\end{array}\right]\left\{\begin{array}{c}\frac{\partial(\cdot)}{\partial x}\\ \frac{\partial(\cdot)}{\partial y}\end{array}\right\}\end{aligned} \tag{5.1.5}$$

or

$$\frac{\partial(\cdot)}{\partial\boldsymbol{\xi}} = \mathbf{J}^T\frac{\partial(\cdot)}{\partial\mathbf{x}}\,. \tag{5.1.6}$$

It should be noted that only the x and y components are included in the above relationship for the partial derivatives. This is a consequence of assuming that the element represents a best fit of the warped quadrilateral in the (x,y)-plane.

If the z-coordinate is neglected the relationship between (x,y) and (ξ,η) is isoparametric and the inverse relation can be formed as

$$\left\{\begin{array}{c}\frac{\partial(\cdot)}{\partial x}\\ \frac{\partial(\cdot)}{\partial y}\end{array}\right\} = \left[\begin{array}{cc}J^{-T}_{x\xi} & J^{-T}_{x\eta}\\ J^{-T}_{y\xi} & J^{-T}_{y\eta}\end{array}\right]\left\{\begin{array}{c}\frac{\partial(\cdot)}{\partial\xi}\\ \frac{\partial(\cdot)}{\partial\eta}\end{array}\right\}. \tag{5.1.7}$$

5.1.1 Geometric quantities for a flat quadrilateral element.

By defining l_{ij} to be length of side edge ij one obtains

$$l_{ij} = \sqrt{x_{ji}^2 + y_{ji}^2}\,. \tag{5.1.8}$$

The unit vector $\mathbf{s}_{ij}$ along side ij and the outward normal vector $\mathbf{n}_{ij}$ of side ij can then be defined as

$$\mathbf{s}_{ij} = \left\{\begin{array}{c}s_{ix}\\ s_{iy}\\ 0\end{array}\right\} = \frac{1}{l_{ij}}\left\{\begin{array}{c}x_{ji}\\ y_{ji}\\ 0\end{array}\right\} \qquad \text{and} \qquad \mathbf{n}_{ij} = \left\{\begin{array}{c}n_{ix}\\ n_{iy}\\ 0\end{array}\right\} = \left\{\begin{array}{c}-s_{iy}\\ s_{ix}\\ 0\end{array}\right\}. \tag{5.1.9}$$

5.2 The quadrilateral membrane element.

Nygård [00] developed a 4-node membrane element with drilling degrees of freedom based on the Free Formulation, which is called the FFQ element. The element has given accurate results for plane membrane problems. Unfortunately, the element is computationally expensive because the formation of each element stiffness requires the numerical inversion of a 12×12 matrix. The goal of the present development is to construct a 4-node membrane element with the same freedom configuration and similar accuracy as the FFQ, but that avoids those expensive matrix inversion.

Recall that element stiffness of the ANDES element is the sum of the basic and higher order contributions:

$$\mathbf{K} = \mathbf{K}_b + \mathbf{K}_h = \frac{1}{A}\mathbf{L}\mathbf{C}\mathbf{L}^T + \int_A \mathbf{B}_h^T \mathbf{C}\mathbf{B}_h \, dA \, . \tag{5.2.1}$$

These matrices are now developed for the membrane component.

5.2.1 Basic stiffness.

The basic stiffness for the membrane element is developed by lumping the constant stress state over side edges to consistent nodal forces at the neighboring nodes according to a boundary displacement field. When the boundary displacement field is defined so that interelement compatibility is satisfied, pairwise cancelation of nodal forces for a constant stress state is assured, and thus satisfaction of the Individual Element Test [00]. In turn, satisfaction of the Individual Element Test ensures that the conventional multi-element Patch Test is passed.

A very successful lumping scheme for membrane stresses was first introduced by Bergan and Felippa [00] in the paper describing the triangular membrane FF element with drilling degrees of freedoms. This procedure has since been used by Nygård [00] and Militello [00].

The presentation here rewrites the lumping matrix, in terms of nodal submatrices. The expressions of the lumping matrix thus becomes valid for elements of arbitrary number of corner nodes.

It is convenient to order the visible degrees of freedom as translations along x, y and drilling rotation about z-axis for each node. This gives the lumping of the constant stress $\boldsymbol{\sigma}$ state to nodal forces $\mathbf{f}$ as

$$\mathbf{f} = \mathbf{L}\boldsymbol{\sigma} \qquad \text{where} \qquad \boldsymbol{\sigma} = \left\{ \begin{array}{c} \sigma_{xx} \\ \sigma_{yy} \\ \tau_{xy} \end{array} \right\}, \tag{5.2.2}$$

$$\mathbf{L} = \begin{bmatrix} \mathbf{L}_1 \\ \mathbf{L}_2 \\ \mathbf{L}_3 \\ \mathbf{L}_4 \end{bmatrix} \quad \text{and} \quad \mathbf{f} = \begin{Bmatrix} \mathbf{f}_1 \\ \mathbf{f}_2 \\ \mathbf{f}_3 \\ \mathbf{f}_4 \end{Bmatrix} \quad \text{where} \quad \mathbf{f}_i = \begin{Bmatrix} f_{xi} \\ f_{y_i} \\ m_{zi} \end{Bmatrix}. \tag{5.2.3}$$

By using the Hermitian beam shape function for a side edge one obtains a boundary displacement field that is compatible between adjacent elements because the displacements along an edge are only functions of the end nodes freedoms. This again gives a lumping matrix $\mathbf{L}$ where each nodal contribution $\mathbf{L}_j$ is only a function of its adjoining side edges ij and jk:

$$\mathbf{L}_j = \frac{1}{2} \begin{bmatrix} y_{ki} & 0 & -x_{ki} \\ 0 & -x_{ki} & y_{ki} \\ \frac{\alpha}{6}(y_{ij}^2 - y_{kj}^2) & \frac{\alpha}{6}(x_{ij}^2 - x_{kj}^2) & \frac{\alpha}{3}(x_{kj}y_{kj} - x_{ij}y_{ij}) \end{bmatrix}. \tag{5.2.4}$$

The nodal indices (i, j, k, l) for a four node element undergo cyclic permutations of $(1, 2, 3, 4)$ in the equation above. Factor α represents a scaling of the contributions of the drilling freedom to the normal boundary displacements; see [00] for details.

5.2.2 Higher order stiffness.

To construct $\mathbf{K}_h$ a set of higher order degrees of freedoms that vanish for rigid body and constant strain states is constructed.

Higher order degrees of freedom.
The 12 visible nodal degrees of freedom v_x, v_y and θ for each node are ordered in an element displacement vector $\mathbf{v}$ as

$$\mathbf{v} = \begin{Bmatrix} \mathbf{v}_x \\ \mathbf{v}_y \\ \boldsymbol{\theta} \end{Bmatrix}, \quad \text{where} \quad \begin{aligned} \mathbf{v}_x^T &= [\, v_{x1} \quad v_{x2} \quad v_{x3} \quad v_{x4} \,], \\ \mathbf{v}_y^T &= [\, v_{y1} \quad v_{y2} \quad v_{y3} \quad v_{y4} \,], \\ \boldsymbol{\theta}^T &= [\, \theta_1 \quad \theta_2 \quad \theta_3 \quad \theta_4 \,]. \end{aligned} \tag{5.2.5}$$

The correct rank of the element stiffness matrix for the quadrilateral membrane element is 9, coming from 12 degrees of freedom minus 3 rigid body modes. The basic stiffness gives is rank 3 from the 3 constant strain modes. The higher order stiffness must therefore be a rank 6 matrix. This can be conveniently achieved by introducing 6 higher order "intrinsic" degrees of freedom, which are collected in a vector $\tilde{\mathbf{v}}$ defined below.

Experience from the 3-node ANDES membrane element with drilling degrees of freedom [00] and the 4-node ANDES tetrahedron solid element with

rotational degrees of freedom [00], suggests using the hierarchical rotations $\tilde{\boldsymbol{\theta}}$ as higher order degrees of freedom:

$$\tilde{\boldsymbol{\theta}} = \boldsymbol{\theta} - \boldsymbol{\theta}_0 \ , \qquad \boldsymbol{\theta}_0^T = [\, \theta_0 \quad \theta_0 \quad \theta_0 \quad \theta_0 \,] \, , \tag{5.2.6}$$

where the subtracted θ_0 represents the overall or mean rotation of the element, associated with rigid body and constant strain rotation motions. Furthermore, splitting the hierarchical rotations into their mean and deviatoric parts as

$$\tilde{\boldsymbol{\theta}} = \bar{\boldsymbol{\theta}} + \boldsymbol{\theta}', \qquad \bar{\boldsymbol{\theta}}^T = [\, \bar{\theta} \quad \bar{\theta} \quad \bar{\theta} \quad \bar{\theta} \,] \, , \tag{5.2.7}$$

has the advantage of singling out the often troublesome "drilling mode", or "torsional mode", where all the drilling node rotations take the same value with all the other degrees of freedom being zero.

Unfortunately, the hierarchical rotations give only 4 higher order degrees of freedom and at most a rank 4 update of the stiffness matrix. Two more higher order degrees of freedom must be found. The element has 8 translational degrees of freedom represented by $\mathbf{v}_x$ and $\mathbf{v}_y$. The 3 rigid body and 3 constant strain modes can all be described by the translational degrees of freedom. There are still 2 higher order modes which can be described by the translational degrees of freedom. These two modes must be recognized so as to associate two higher order degrees of freedom with them. The amplitudes of the six higher order degrees of freedom are then represented as

$$\tilde{\mathbf{v}}^T = [\, \theta_1' \quad \theta_2' \quad \theta_3' \quad \theta_4' \quad \bar{\theta} \quad \alpha_1 \quad \alpha_2 \,] \, , \tag{5.2.8}$$

where α_1 and α_2 are associated with the two higher order translational modes. Although 7 degrees of freedom appear in this vector, the hierarchical rotation constraint

$$\sum_{i=1}^{4} \theta_i' = 0 \tag{5.2.9}$$

reduces (5.2.8) effectively to six independent components.

Higher order rotational degrees of freedom.
θ_0 is evaluated as the rotation of the bi-linear quadrilateral computed at the element center given by $(\xi = 0, \eta = 0)$, and is function of the translational degrees of freedom only:

$$\theta_0 = \frac{1}{2}(\frac{\partial v}{\partial x} - \frac{\partial u}{\partial y}) = \frac{1}{2}\,[\,-\mathbf{N}_{,y} \quad \mathbf{N}_{,x}\,] \left\{ \begin{array}{c} \mathbf{v}_x \\ \mathbf{v}_y \end{array} \right\}. \tag{5.2.10}$$

By using the partial derivative expressions in equation (5.1.7) one obtains the expressions for the rigid body and constant strain rotation as

$$\begin{aligned} -\mathbf{N}_{,y} &= -(J_{y\xi}^{-T}\mathbf{N}_{,\xi} + J_{y\eta}^{-T}\mathbf{N}_{,\eta}) = \frac{1}{16|\mathbf{J}|}\,[\,x_{24} \quad x_{31} \quad x_{42} \quad x_{13}\,], \\ \mathbf{N}_{,x} &= -(J_{x\xi}^{-T}\mathbf{N}_{,\xi} + J_{x\eta}^{-T}\mathbf{N}_{,\eta}) = \frac{1}{16|\mathbf{J}|}\,[\,y_{24} \quad y_{31} \quad y_{42} \quad y_{13}\,], \end{aligned} \tag{5.2.11}$$

where

$$|\mathbf{J}| = \frac{1}{8}((x_1y_2 - x_2y_1) + (x_2y_3 - x_3y_2) + (x_3y_4 - x_4y_3) + (x_4y_1 - x_1y_4)). \tag{5.2.12}$$

The higher order rotational degrees of freedom θ_h can be expressed in terms of the visible degrees of freedoms as

$$\boldsymbol{\theta}_h = \mathbf{H}_{\theta v}\mathbf{v}, \qquad \boldsymbol{\theta}_h^T = [\,\theta_1' \quad \theta_2' \quad \theta_3' \quad \theta_4' \quad \bar{\theta}\,], \tag{5.2.13}$$

$$\mathbf{H}_{\theta v} = \begin{bmatrix} 0 & 0 & 0 & 0 & 0 & 0 & 0 & 0 & \frac{3}{4} & -\frac{1}{4} & -\frac{1}{4} & -\frac{1}{4} \\ 0 & 0 & 0 & 0 & 0 & 0 & 0 & 0 & -\frac{1}{4} & \frac{3}{4} & -\frac{1}{4} & -\frac{1}{4} \\ 0 & 0 & 0 & 0 & 0 & 0 & 0 & 0 & -\frac{1}{4} & -\frac{1}{4} & \frac{3}{4} & -\frac{1}{4} \\ 0 & 0 & 0 & 0 & 0 & 0 & 0 & 0 & -\frac{1}{4} & -\frac{1}{4} & -\frac{1}{4} & \frac{3}{4} \\ \frac{x_{42}}{f} & \frac{x_{13}}{f} & \frac{x_{24}}{f} & \frac{x_{31}}{f} & \frac{y_{42}}{f} & \frac{y_{13}}{f} & \frac{y_{24}}{f} & \frac{y_{31}}{f} & \frac{1}{4} & \frac{1}{4} & \frac{1}{4} & \frac{1}{4} \end{bmatrix} \tag{5.2.14}$$

and $f = 16|\mathbf{J}|$.

Higher order translational degrees of freedom.
The translational degrees of freedom can be split into rigid body and constant strain displacements and higher order displacements:

$$\mathbf{v} = \mathbf{v}_{rc} + \mathbf{v}_h \quad \text{where} \quad \mathbf{v} = \left\{ \begin{array}{c} \mathbf{v}_x \\ \mathbf{v}_y \end{array} \right\}. \tag{5.2.15}$$

$\mathbf{v}_{rc}$ can be written as a linear combination of the rc-modes as

$$\mathbf{v}_{rc} = \mathbf{R}\mathbf{a} \quad \text{with} \quad \mathbf{R} = [\, \mathbf{r}_x \quad \mathbf{r}_y \quad \mathbf{r}_{\theta_z} \quad \mathbf{c}_{\epsilon_{xx}} \quad \mathbf{c}_{\epsilon_{yy}} \quad \mathbf{c}_{\epsilon_{xy}} \,], \tag{5.2.16}$$

where $\mathbf{r}_x$, $\mathbf{r}_y$ and $\mathbf{r}_{\theta_z}$ are the rigid translations in the x and y directions, and the rigid rotation about the z axis, respectively. $\mathbf{c}_{\epsilon_{xx}}$, $\mathbf{c}_{\epsilon_{xx}}$ and $\mathbf{c}_{\epsilon_{xx}}$ are the constant strain displacement modes. By combining equations (5.2.15) and (5.2.16), and requiring that the higher order displacement vector be orthogonal to the rc-modes, that is $\mathbf{R}^T\mathbf{v}_h = \mathbf{0}$, one obtains

$$\mathbf{R}^T\mathbf{v} = \mathbf{R}^T\mathbf{R}\mathbf{a} + \mathbf{R}^T\mathbf{v}_h \quad \Rightarrow \quad \mathbf{a} = (\mathbf{R}^T\mathbf{R})^{-1}\mathbf{R}^T\mathbf{v}\,. \tag{5.2.17}$$

On the basis of this relation two projector matrices $\mathbf{P}_{rc}$ and $\mathbf{P}_h$ that project the displacement vector $\mathbf{v}$ on the rc and h subspaces, respectively, can be constructed:

$$\begin{array}{l} \mathbf{v}_{rc} = \mathbf{P}_{rc}\mathbf{v}\,, \\ \mathbf{v}_h = \mathbf{P}_h\mathbf{v}\,, \end{array} \quad \text{where} \quad \begin{array}{l} \mathbf{P}_{rc} = \mathbf{R}(\mathbf{R}^T\mathbf{R})^{-1}\mathbf{R}^T\,, \\ \mathbf{P}_h = \mathbf{I} - \mathbf{R}(\mathbf{R}^T\mathbf{R})^{-1}\mathbf{R}^T\,. \end{array} \tag{5.2.18}$$

The higher order translational modes can now be found either as the null-space of $\mathbf{P}_{rc}$, or as eigenvectors of $\mathbf{P}_h$ with associated eigenvalues equal to one, that is $\mathbf{P}_h\mathbf{v}_h = \mathbf{v}_h$. The latter scheme is the simpler one because the projector matrices enjoy the property $\mathbf{P}\mathbf{P} = \mathbf{P}$. Every column in $\mathbf{P}_h$ is thus its own eigenvector with eigenvalue one, and a higher order mode.

To write down these higher order modes in compact form it is convenient to expresses the vector that goes from the element centroid to the nodes $\mathbf{r}_i$ with respect to the local coordinate system $(\mathbf{g}_\xi, \mathbf{g}_\eta)$. These base vectors are the ξ- and η- gradient vectors computed at the element center according to equation (5.1.4). The nodal vector $\mathbf{r}_i$ can thus be expressed as

$$\mathbf{r}_i = \left\{ \begin{array}{c} x_i \\ y_i \end{array} \right\} = [\, \mathbf{g}_\xi \quad \mathbf{g}_\eta \,] \left\{ \begin{array}{c} \xi_i \\ \eta_i \end{array} \right\}. \tag{5.2.19}$$

The nodal coordinates ξ_i and η_i in the $(\mathbf{g}_\xi, \mathbf{g}_\eta)$ coordinate system are then obtained from

$$\left\{ \begin{array}{c} \xi_i \\ \eta_i \end{array} \right\} = \mathbf{T}_\xi \left\{ \begin{array}{c} x_i \\ y_i \end{array} \right\}, \qquad \mathbf{T}_\xi = \mathbf{J}^{-1} = [\, \mathbf{g}_\xi \quad \mathbf{g}_\eta \,]^{-1} \,. \tag{5.2.20}$$

The higher order translational mode is then given by

$$\mathbf{v}_h = \left\{ \begin{array}{c} \varsigma_3 \\ \varsigma_4 \\ \varsigma_1 \\ \varsigma_2 \end{array} \right\} = \left\{ \begin{array}{c} \xi_3\eta_3 - a \\ \xi_4\eta_4 - a \\ \xi_1\eta_1 - a \\ \xi_2\eta_2 - a \end{array} \right\}, \qquad a = \frac{1}{4}\sum_{i=1}^{4} \xi_i\eta_i \,. \tag{5.2.21}$$

The higher order translational degrees of freedom are the components along this higher order mode for the x and y nodal displacements $\mathbf{v}_x$ and $\mathbf{v}_y$ respectively. Expressed in term of the visible degrees of freedom this becomes

$$\tilde{\mathbf{v}}_t = \mathbf{H}_{tv}\mathbf{v} \,, \tag{5.2.22}$$

$$\left\{ \begin{array}{c} \tilde{v}_x \\ \tilde{v}_y \end{array} \right\} = \left[\begin{array}{cccccccccccc} \varsigma_3 & \varsigma_4 & \varsigma_1 & \varsigma_2 & 0 & 0 & 0 & 0 & 0 & 0 & 0 & 0 \\ 0 & 0 & 0 & 0 & \varsigma_3 & \varsigma_4 & \varsigma_1 & \varsigma_2 & 0 & 0 & 0 & 0 \end{array} \right] \mathbf{v} \,. \tag{5.2.23}$$

If one defines the higher order translational degrees of freedom to be the higher order translational components along the ξ and η directions the relationship becomes

$$\left\{ \begin{array}{c} \tilde{v}_\xi \\ \tilde{v}_\eta \end{array} \right\} = \left[\begin{array}{cccccccccc} \varsigma_3 s_{\xi x} & \varsigma_4 s_{\xi x} & \varsigma_1 s_{\xi x} & \varsigma_2 s_{\xi x} & \varsigma_3 s_{\xi y} & \varsigma_4 s_{\xi y} & \varsigma_1 s_{\xi y} & \varsigma_2 s_{\xi y} & \mathbf{0} \\ \varsigma_3 s_{\eta x} & \varsigma_4 s_{\eta x} & \varsigma_1 s_{\eta x} & \varsigma_2 s_{\eta x} & \varsigma_3 s_{\eta y} & \varsigma_4 s_{\eta y} & \varsigma_1 s_{\eta y} & \varsigma_2 s_{\eta y} & \mathbf{0} \end{array} \right] \mathbf{v} \tag{5.2.24}$$

where $\mathbf{0} = [\, 0 \quad 0 \quad 0 \quad 0 \,]$, and $s_{\xi i}$ and $s_{\eta i}$ denotes the unit vectors along the ξ- and η-directions, respectively:

$$\mathbf{s}_\xi = \left\{ \begin{array}{c} s_{\xi x} \\ s_{\xi y} \end{array} \right\}, \qquad \mathbf{s}_\eta = \left\{ \begin{array}{c} s_{\eta x} \\ s_{\eta y} \end{array} \right\}. \tag{5.2.25}$$

The total higher order degrees of freedom vector $\tilde{\mathbf{v}}$ can then be obtained from the visible degrees of freedom $\mathbf{v}$ as

$$\tilde{\mathbf{v}} = \mathbf{H}\mathbf{v} \quad \text{where} \quad \mathbf{H} = \left[\begin{array}{c} \mathbf{H}_{\theta v} \\ \mathbf{H}_{vt} \end{array} \right] \quad \text{and} \quad \begin{array}{l} \tilde{\mathbf{v}}^T = [\, \theta'_1 \quad \theta'_2 \quad \theta'_3 \quad \theta'_4 \quad \bar{\theta} \quad \tilde{v}_\xi \quad \tilde{v}_\eta \,] \\ \mathbf{v}^T = [\, \mathbf{v}_x^T \quad \mathbf{v}_y^T \quad \boldsymbol{\theta}^T \,] \,. \end{array} \tag{5.2.26}$$

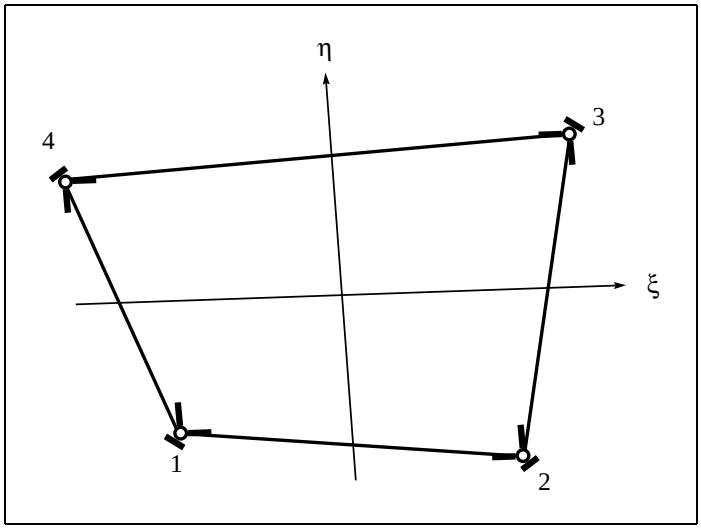

Figure 5.1. Nodal strain gages for membrane.

Higher order strains.
The distribution of higher order strains is expressed in terms of natural strain gage readings. The strain gage locations are placed at the 4 nodes (quadrilateral corners). Readings along three directions are required. These directions are: the ξ and η axis (quadrilateral medians) and the diagonal passing through the neighboring nodes. See Figure 4.1.

The nodal natural strain readings are thus defined as

$$\boldsymbol{\epsilon}_1 = \left\{ \begin{array}{c} \epsilon_\xi \\ \epsilon_\eta \\ \epsilon_{24} \end{array} \right\}, \quad \boldsymbol{\epsilon}_2 = \left\{ \begin{array}{c} \epsilon_\xi \\ \epsilon_\eta \\ \epsilon_{13} \end{array} \right\}, \quad \boldsymbol{\epsilon}_3 = \left\{ \begin{array}{c} \epsilon_\xi \\ \epsilon_\eta \\ \epsilon_{24} \end{array} \right\}, \quad \boldsymbol{\epsilon}_4 = \left\{ \begin{array}{c} \epsilon_\xi \\ \epsilon_\eta \\ \epsilon_{13} \end{array} \right\}. \qquad (5.2.27)$$

The next step is to connect these readings to the higher order degrees of freedom. This can be done by defining a generic template

$$\boldsymbol{\epsilon}_i = \mathbf{Q}_i \tilde{\mathbf{v}} \,, \qquad (5.2.28)$$

where $\mathbf{Q}_i$ are 3×7 matrices. These templates are worked out below.

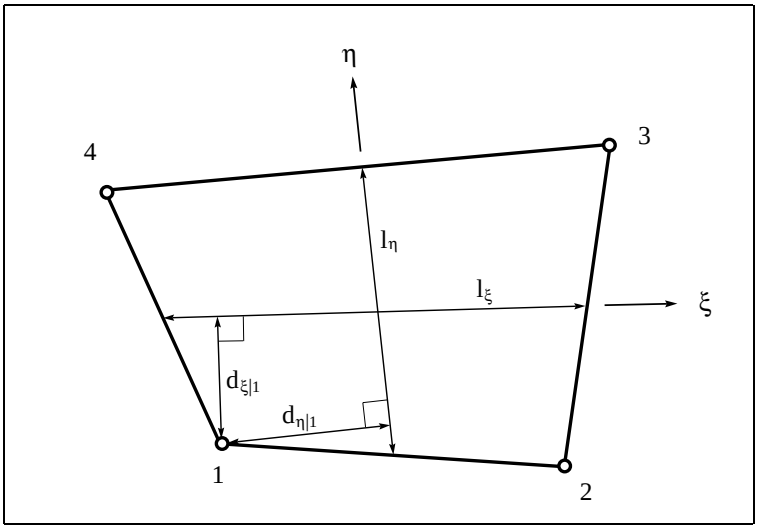

Figure 5.2. Geometric dimensions for a quadrilateral element.

Higher order bending strain field.
The main displacement and strain mode that the field is trying to match is the pure bending of the element along an arbitrary direction. The bending strain field is associated with the higher order degrees of freedom θ_i', $\tilde{v}_\xi$ and $\tilde{v}_\eta$. If one considers pure bending of the element along the ξ direction, it seems intuitive that the ξ strain should be proportional to the distance d_ξ from the ξ-axis. The ξ strain should also be proportional to the curvature along the ξ-axis. In terms of the rotational degrees of freedoms this curvature will have the form $\Delta\theta/l_\xi$ where l_ξ is the element length along the ξ-axis. The ξ strain thus gets coefficients of the form d_ξ/l_ξ associated with the rotational degrees of freedom. Following a similar reasoning for the η strains the strain distribution factors associated with the ξ and η strains are established to be

$$\chi_{\xi|i} = \frac{d_{\xi|i}}{l_\xi} \,, \qquad \chi_{\eta|i} = \frac{d_{\eta|i}}{l_\eta} \,, \tag{5.2.29}$$

where

$$d_{\xi|i} = \sqrt{(\mathbf{r}_i \times \mathbf{s}_\xi)\cdot(\mathbf{r}_i \times \mathbf{s}_\xi)} \,, \quad l_\xi = \sqrt{\mathbf{r}_\xi \cdot \mathbf{r}_\xi} \,, \quad \mathbf{r}_\xi = \frac{1}{2}(\mathbf{r}_2 + \mathbf{r}_3 - \mathbf{r}_1 - \mathbf{r}_4) \,,$$

$$d_{\eta|i} = \sqrt{(\mathbf{r}_i \times \mathbf{s}_\eta)\cdot(\mathbf{r}_i \times \mathbf{s}_\eta)} \,, \quad l_\eta = \sqrt{\mathbf{r}_\eta \cdot \mathbf{r}_\eta} \,, \quad \mathbf{r}_\eta = \frac{1}{2}(\mathbf{r}_3 + \mathbf{r}_4 - \mathbf{r}_1 - \mathbf{r}_2) \,.$$

The quantities $d_{\xi|i}$, $d_{\eta|i}$, l_ξ and l_η are illustrated in Figure 4.2.

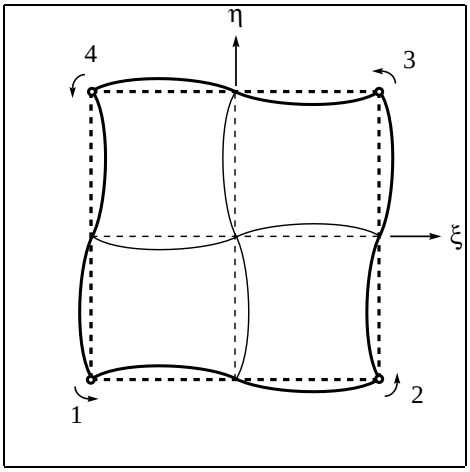

Figure 5.3. Torsional mode for four node membrane element.

The strain distribution sensed by the diagonal strain gages are similarly assumed to be proportional to the curvature along the diagonal, and proportional to the distance from the diagonal as

$$\chi_{24} = \frac{d_{24}}{2l_{24}} , \qquad \chi_{13} = \frac{d_{13}}{2l_{13}} , \tag{5.2.30}$$

where

$$d_{24} = \sqrt{(\mathbf{r}_{31} \times \mathbf{e}_{24}) \cdot (\mathbf{r}_{13} \times \mathbf{e}_{24})} , \quad l_{24} = \sqrt{\mathbf{r}_{24} \cdot \mathbf{r}_{24}} , \quad \mathbf{r}_{24} = (\mathbf{r}_2 - \mathbf{r}_4) ,$$

$$d_{13} = \sqrt{(\mathbf{r}_{31} \times \mathbf{e}_{24}) \cdot (\mathbf{r}_{13} \times \mathbf{e}_{24})} , \quad l_{13} = \sqrt{\mathbf{r}_{13} \cdot \mathbf{r}_{13}} , \quad \mathbf{r}_{13} = (\mathbf{r}_1 - \mathbf{r}_3) .$$

Torsional strain field.
The torsional strain field is associated to the $\bar{\theta}$ higher order degree of freedom. As a guide for the construction of this strain field one can use the torsional displacement mode illustrated in Figure 4.3. This figure indicates that this displacement mode should not induce shear strains, and that ϵ_ξ should be positive in 1st and 3rd quadrants and negative in 2nd and 4th. Similarly, ϵ_η should be positive in 2nd and 4th, and negative in 1st and 3rd quadrants. A simplified strain distribution function for the strains ϵ_ξ and ϵ_η can thus be $N_t = \xi\eta$.

With a unit rotation at all the nodes, the maximum displacement in the ξ direction, u_ξ, will be proportional to the length l_η. Since the strain ϵ_ξ is the gradient of the displacement u_ξ in the ξ direction this strain will be proportional to $1/l_\xi$. The torsional strain field is thus assumed to be

$$\epsilon_\xi = \alpha \frac{l_\eta}{l_\xi} \xi\eta = \alpha \chi_{\xi t}\, \xi\eta, \qquad \epsilon_\eta = -\alpha \frac{l_\xi}{l_\eta} \xi\eta = -\alpha \chi_{\eta t}\, \xi\eta. \tag{5.2.31}$$

Generic nodal strain templates.
With the strain assumptions just described, the nodal strain gage readings can be written down as

$$\mathbf{Q}_1 = \tag{5.2.32}$$
$$\begin{bmatrix} \rho_1\chi_{\xi|1} & \rho_2\chi_{\xi|1} & \rho_3\chi_{\xi|1} & \rho_4\chi_{\xi|1} & \alpha\chi_{\xi t} & -\beta_1\frac{\chi_{\xi|1}}{\bar{\chi}_\xi l_\xi} & 0 \\ -\rho_1\chi_{\eta|1} & -\rho_4\chi_{\eta|1} & -\rho_3\chi_{\eta|1} & -\rho_2\chi_{\eta|1} & -\alpha\chi_{\eta t} & 0 & -\beta_1\frac{\chi_{\eta|1}}{\bar{\chi}_\eta l_\eta} \\ \rho_5\chi_{24} & \rho_6\chi_{24} & \rho_7\chi_{24} & \rho_8\chi_{24} & 0 & \beta_2\frac{c_{24\xi}}{l_{24}} & -\beta_2\frac{c_{24\eta}}{l_{24}} \end{bmatrix},$$

$$\mathbf{Q}_2 = \tag{5.2.33}$$
$$\begin{bmatrix} -\rho_2\chi_{\xi|2} & -\rho_1\chi_{\xi|2} & -\rho_4\chi_{\xi|2} & -\rho_3\chi_{\xi|2} & -\alpha\chi_{\xi t} & -\beta_1\frac{\chi_{\xi|2}}{\bar{\chi}_\xi l_\xi} & 0 \\ \rho_4\chi_{\eta|2} & \rho_1\chi_{\eta|2} & \rho_2\chi_{\eta|2} & \rho_3\chi_{\eta|2} & \alpha\chi_{\eta t} & 0 & \beta_1\frac{\chi_{\eta|2}}{\bar{\chi}_\eta l_\eta} \\ \rho_8\chi_{13} & \rho_5\chi_{13} & \rho_6\chi_{13} & \rho_7\chi_{13} & 0 & -\beta_2\frac{c_{13\xi}}{l_{13}} & \beta_2\frac{c_{13\eta}}{l_{13}} \end{bmatrix},$$

$$\mathbf{Q}_3 = \tag{5.2.34}$$
$$\begin{bmatrix} \rho_3\chi_{\xi|3} & \rho_4\chi_{\xi|3} & \rho_1\chi_{\xi|3} & \rho_2\chi_{\xi|3} & \alpha\chi_{\xi t} & \beta_1\frac{\chi_{\xi|3}}{\bar{\chi}_\xi l_\xi} & 0 \\ -\rho_3\chi_{\eta|3} & -\rho_2\chi_{\eta|3} & -\rho_1\chi_{\eta|3} & -\rho_4\chi_{\eta|3} & -\alpha\chi_{\eta t} & 0 & \frac{\beta_1\chi_{\eta|3}}{\bar{\chi}_\eta l_\eta} \\ \rho_7\chi_{13} & \rho_8\chi_{13} & \rho_5\chi_{13} & \rho_6\chi_{13} & 0 & -\beta_2\frac{c_{13\xi}}{l_{13}} & \beta_2\frac{c_{13\eta}}{l_{13}} \end{bmatrix},$$

$$\mathbf{Q}_4 = \tag{5.2.35}$$
$$\begin{bmatrix} -\rho_4\chi_{\xi|4} & -\rho_3\chi_{\xi|4} & -\rho_2\chi_{\xi|4} & -\rho_1\chi_{\xi|4} & -\alpha\chi_{\xi t} & \beta_1\frac{\chi_{\xi|4}}{\bar{\chi}_\xi l_\xi} & 0 \\ \rho_2\chi_{\eta|4} & \rho_3\chi_{\eta|4} & \rho_4\chi_{\eta|4} & \rho_1\chi_{\eta|4} & \alpha\chi_{\eta t} & 0 & -\beta_1\frac{\chi_{\eta|4}}{\bar{\chi}_\eta l_\eta} \\ \rho_6\chi_{13} & \rho_7\chi_{13} & \rho_8\chi_{13} & \rho_5\chi_{13} & 0 & \beta_2\frac{c_{13\xi}}{l_{13}} & -\beta_2\frac{c_{13\eta}}{l_{13}} \end{bmatrix},$$

where $c_{13\xi} = \mathbf{s}_{13}^T\mathbf{s}_\xi$, $c_{13\eta} = \mathbf{s}_{13}^T\mathbf{s}_\eta$, $c_{24\xi} = \mathbf{s}_{24}^T\mathbf{s}_\xi$ and $c_{24\eta} = \mathbf{s}_{24}^T\mathbf{s}_\eta$.

The cartesian strain displacement matrices at the nodes are obtained by the transformations

$$\begin{aligned} \mathbf{B}_{h1} &= \mathbf{T}_{13}\mathbf{Q}_1 \ , \\ \mathbf{B}_{h3} &= \mathbf{T}_{13}\mathbf{Q}_3 \ , \end{aligned} \quad \text{where} \quad \mathbf{T}_{13}^{-1} = \begin{bmatrix} {s_{\xi}}_x^2 & {s_{\xi}}_y^2 & s_{\xi_x}s_{\xi_y} \\ {s_{\eta}}_x^2 & {s_{\eta}}_y^2 & s_{\eta_x}s_{\eta_y} \\ {s_{24}}_x^2 & {s_{24}}_y^2 & s_{24_x}s_{24_y} \end{bmatrix}, \tag{5.2.36}$$

$$\begin{aligned} \mathbf{B}_{h2} &= \mathbf{T}_{24}\mathbf{Q}_2 \ , \\ \mathbf{B}_{h4} &= \mathbf{T}_{24}\mathbf{Q}_4 \ , \end{aligned} \quad \text{where} \quad \mathbf{T}_{24}^{-1} = \begin{bmatrix} {s_{\xi}}_x^2 & {s_{\xi}}_y^2 & s_{\xi_x}s_{\xi_y} \\ {s_{\eta}}_x^2 & {s_{\eta}}_y^2 & s_{\eta_x}s_{\eta_y} \\ {s_{13}}_x^2 & {s_{13}}_y^2 & s_{13_x}s_{13_y} \end{bmatrix}. \tag{5.2.37}$$

A higher order strain field over the element can now be obtained by interpolating the nodal Cartesian strains by use of the bi-linear shape functions defined in (5.1.3).

$$\begin{aligned}\mathbf{B}_h(\xi,\eta) = \quad & (1-\xi)(1-\eta)\mathbf{B}_{h1} + (1+\xi)(1-\eta)\mathbf{B}_{h2} \\ & +(1+\xi)(1+\eta)\mathbf{B}_{h3} + (1-\xi)(1+\eta)\mathbf{B}_{h4} \ .\end{aligned} \tag{5.2.38}$$

Interpolation of these nodal strains does not automatically give a deviatoric higher order strain field. Such a condition can be achieved by subtracting the mean strain values:

$$\mathbf{B}_d(\xi,\eta) = \mathbf{B}_h(\xi,\eta) - \bar{\mathbf{B}}_h \quad \text{where} \quad \bar{\mathbf{B}}_h = \int_A \mathbf{B}(\xi,\eta)\, dA \ . \tag{5.2.39}$$

Optimal coefficients for the strain computation.
When computing the strain displacement expressions symbolically using Mathematica, the contributions of the different coefficients ρ_i and β_i were evaluated with respect to certain higher order strain modes. Based on pure bending of rectangular element shapes the following dependencies between the coefficients were obtained:

$$\begin{aligned} &\rho_2 = -\rho_1 \ , \qquad \rho_3 = \rho_2 \ , \qquad \rho_4 = \rho_1 \ , \\ &\rho_6 = \beta_1 - \rho_1 \ , \qquad \beta_1 = \frac{1}{2} + \rho_1 \ , \\ &\rho_8 = -\rho_6 \ , \qquad \rho_5 = \rho_7 = \beta_2 = 0 \ . \end{aligned} \tag{5.2.40}$$

As seen this makes all the coefficients a function of ρ_1. Optimizing ρ_1 with respect to irregular meshes for the cantilever described in the numerical section suggests $\rho_1 = 0.1$, and the following set of optimal coefficients:

$$\begin{array}{cccc} \rho_1 = 0.1 & \rho_2 = -0.1 & \rho_3 = -0.1 & \rho_4 = 0.1 \\ \rho_5 = 0.0 & \rho_6 = 0.5 & \rho_7 = 0.0 & \rho_8 = -0.5 \\ & \beta_1 = 0.6 & \beta_2 = 0.0 & \end{array} \tag{5.2.41}$$

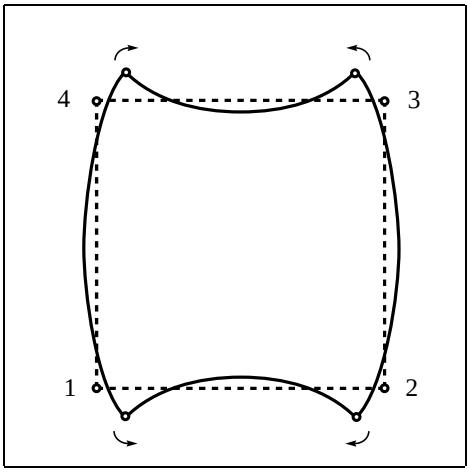

Figure 5.4. Spurious membrane mode for the four node ANDES element.

Stiffness computation for the membrane element.
According to the ANDES formulation the element stiffness is computed as

$$\mathbf{K} = \frac{1}{A}\mathbf{L}\mathbf{C}\mathbf{L}^T + \mathbf{H}^T\tilde{\mathbf{K}}_d\mathbf{H} \quad \text{where} \quad \tilde{\mathbf{K}}_d = \int_A \mathbf{B}_d^T\mathbf{C}\mathbf{B}_d \, dA \, . \tag{5.2.42}$$

Numerical experiments, however, indicate that the element performs better when the element stiffness is computed as

$$\mathbf{K} = \frac{1}{A}\mathbf{L}\mathbf{C}\mathbf{L}^T + \mathbf{H}^T\tilde{\mathbf{K}}_h\mathbf{H} \quad \text{where} \quad \tilde{\mathbf{K}}_h = \int_A \mathbf{B}_h^T\mathbf{C}\mathbf{B}_h \, dA \, , \tag{5.2.43}$$

that is when the non-deviatoric higher order strains are used. This is not strictly justified according to the standard ANDES formulation since the higher order strains displacement matrix $\mathbf{B}_h$ is not energy orthogonal with respect to the constant strain modes for arbitrary element geometries. However, both of the above element stiffness matrices satisfy the Individual Element Test and thus also the conventional Patch Test.

Rank of the stiffness matrix.
Performing an eigenvalue analysis of the element stiffness matrices given in equations (5.2.42) and (5.2.43) it was found that the element has one spurious zero energy mode in addition to the correct three rigid body modes. This spurious mode occurred using a 2×2 Gauss integration rule. It is expected that this spurious mode would disappear with a 3×3 integration rule. For a square element

as shown in Figure 5.4 this spurious mode is defined by the nodal displacement pattern

$$\begin{aligned}\mathbf{v}^T &= [\, v_{x1} \quad v_{x2} \quad v_{x3} \quad v_{x4} \quad v_{y1} \quad v_{y2} \quad v_{y3} \quad v_{y4} \quad \theta_{z1} \quad \theta_{z2} \quad \theta_{z3} \quad \theta_{z4} \,] \\ &= [\ \ 1 \quad -1 \quad -1 \quad\ \ 1 \quad -1 \quad -1 \quad\ \ 1 \quad\ \ 1 \quad\ \ 4 \quad -4 \quad\ \ 4 \quad -4 \,]\,. \end{aligned} \tag{5.2.44}$$

Analysis of a mesh of two elements shows that this the pattern (5.2.44) can not occur in a mesh of more than one element. The spurious mode is then not practically significant for the performance of the element.

5.3 The quadrilateral bending element.

The current approach to deriving the quadrilateral plate bending element utilizes reference lines. Hrennikoff [00] first used this concept for plate modeling where the goal was to come up with a beam framework useful as a model for bending of flat plates.

Park and Stanley [00, 00] used the reference line concept in their development of several plate and shell elements based on the ANS formulation. The reference lines were used to find beam-like curvatures; these curvatures were then used to find the plate curvatures through various Assumed Natural Strain distributions. These plate and shell elements were of Mindlin-Reissner type, and the reference lines were treated as Timoshenko beams.

The present element is a Kirchhoff type plate and the reference lines are thus treated like Euler-Bernoulli (or Hermitian) beams.

5.3.1 Basic stiffness.

The basic stiffness for a flat quadrilateral bending element has been developed by extending the triangle element lumping matrices $\mathbf{L}_l$ and $\mathbf{L}_q$ of Militello to four node elements. $\mathbf{L}_l$ and $\mathbf{L}_q$ denotes lumping with respect to a linear and quadratic variation in the normal side rotation respectively.

By ordering the element degrees of freedom as rotation about x and y axis and translation in z direction for each node one obtains the lumped forces from bending as

$$\mathbf{f} = \mathbf{L}_l \boldsymbol{\sigma} \quad \text{or} \quad \mathbf{f} = \mathbf{L}_q \boldsymbol{\sigma} \quad \text{where} \quad \boldsymbol{\sigma} = \begin{Bmatrix} m_{xx} \\ m_{yy} \\ m_{xy} \end{Bmatrix}, \tag{5.3.1}$$

$$\mathbf{L}_l = \begin{bmatrix} \mathbf{L}_{l1} \\ \mathbf{L}_{l2} \\ \mathbf{L}_{l3} \\ \mathbf{L}_{l4} \end{bmatrix}, \qquad \mathbf{L}_q = \begin{bmatrix} \mathbf{L}_{q1} \\ \mathbf{L}_{q2} \\ \mathbf{L}_{q3} \\ \mathbf{L}_{q4} \end{bmatrix} \tag{5.3.2}$$

and

$$\mathbf{f} = \left\{ \begin{array}{c} \mathbf{f}_1 \\ \mathbf{f}_1 \\ \mathbf{f}_1 \\ \mathbf{f}_1 \end{array} \right\} \quad \text{where} \quad \mathbf{f}_i = \left\{ \begin{array}{c} m_x \\ m_y \\ f_z \end{array} \right\}. \tag{5.3.3}$$

The lumped node forces at a node j given by lumping matrix $\mathbf{L}_j$, receive contributions from the moments from adjoining sides ij and jk. The lumped force vector at a node j is thus a function of the coordinates of the sides ij and jk only. With linear interpolation of the normal and tangential rotations along a side the lumping matrix becomes

$$\mathbf{L}_{lj} = \frac{1}{2} \left[\begin{array}{ccc} 0 & 0 & 0 \\ 0 & -x_{ki} & y_{ki} \\ -y_{ki} & 0 & -x_{ki} \end{array} \right], \tag{5.3.4}$$

where superscript l denotes linear variation of normal rotation. If the normal rotation is assumed to vary quadratically in accordance to Hermitian interpolation whereas and the tangential rotation still varies linearly the lumping matrix becomes

$$\mathbf{L}_{qj} = \left[\begin{array}{ccc} -c_{jk}s_{jk} + c_{ij}s_{ij} & c_{jk}s_{jk} - c_{ij}s_{ij} & -(s_{jk}^2 - c_{jk}^2) + (s_{ij}^2 + s_{ij}^2) \\ \frac{1}{2}(s_{jk}^2 x_{jk} + s_{ij}^2 x_{ij}) & \frac{1}{2}(c_{jk}^2 x_{jk} + c_{ij}^2 x_{ij}) & -c_{jk}^2 y_{jk} - c_{ij}^2 y_{ij} \\ \frac{1}{2}(s_{jk}^2 y_{jk} + s_{ij}^2 y_{ij}) & \frac{1}{2}(c_{jk}^2 y_{jk} + c_{ij}^2 y_{ij}) & -s_{jk}^2 x_{jk} - s_{ij}^2 x_{ij} \end{array} \right] \tag{5.3.5}$$

where superscript q is used to denote quadratic variation of normal rotations. The nodal indices (i, j, k, l) in the equations above undergo cyclic permutations of $(1, 2, 3, 4)$ as for the membrane lumping.

5.3.2 Higher order stiffness

The higher order stiffness is computed as the deviatoric part of an ANS type element using the Euler-Bernoulli beam as a reference line strain guide.

Nodal curvatures of a Euler-Bernoulli beam.
The transverse displacement of a Euler-Bernoulli beam, written as a function of the nodal displacements and rotations is

$$w = \mathbf{N}_w \mathbf{v}_{bij} \ , \tag{5.3.6}$$

where

$$\mathbf{N}^T = \frac{1}{8} \begin{Bmatrix} 2\,(\ \ 2+\xi)(-1+\xi)^2 \\ l\,(\ \ 1+\xi)(-1+\xi)^2 \\ 2\,(\ \ 2-\xi)(\ \ 1+\xi)^2 \\ l\,(-1+\xi)(\ \ 1+\xi)^2 \end{Bmatrix} \quad \text{and} \quad \mathbf{v}_{bij} = \begin{Bmatrix} w_i \\ \theta_{ni} \\ w_j \\ \theta_{nj} \end{Bmatrix}.$$

The beam curvatures are

$$\kappa = \frac{\partial^2 w}{\partial x^2} = \frac{1}{l^2} \begin{Bmatrix} 6\xi \\ l\,(-1+3\xi) \\ -6\xi \\ l\,(-1+3\xi) \end{Bmatrix} \mathbf{v}_{bij} \ , \tag{5.3.7}$$

The nodal curvatures are then

$$\begin{Bmatrix} \kappa_{ij|i} \\ \kappa_{ij|j} \end{Bmatrix} = \frac{1}{l^2} \begin{bmatrix} -6 & -4l & 6 & -2l \\ 6 & 2l & -6 & 4l \end{bmatrix} \mathbf{v}_{bij} \tag{5.3.8}$$

The nodal displacements of a reference-line from node i to j can be expressed in terms of the visible degrees of freedom at those nodes as

$$\mathbf{v}_{bij} = \mathbf{T}_{vij} \mathbf{v}_{ij} \tag{5.3.9}$$

$$\begin{Bmatrix} w_i \\ \theta_{ni} \\ w_j \\ \theta_{nj} \end{Bmatrix} = \begin{bmatrix} 1 & 0 & 0 & 0 & 0 & 0 \\ 0 & n_{ij_x} & n_{ij_y} & 0 & 0 & 0 \\ 0 & 0 & 0 & 1 & 0 & 0 \\ 0 & 0 & 0 & 0 & n_{ij_x} & n_{ij_y} \end{bmatrix} \begin{Bmatrix} w_i \\ \theta_{xi} \\ \theta_{y_i} \\ w_j \\ \theta_{y_j} \\ \theta_{y_j} \end{Bmatrix}. \tag{5.3.10}$$

The nodal curvatures expressed in terms of the visible dofs at node i and j then become

$$\begin{Bmatrix} \kappa_{ij|i} \\ \kappa_{ij|j} \end{Bmatrix} = \frac{1}{l^2} \begin{bmatrix} -6 & -4l\,n_{ij_x} & -4l\,n_{ij_y} & 6 & -2l\,n_{ij_x} & -2l\,n_{ij_y} \\ 6 & 2l\,n_{ij_x} & 2l\,n_{ij_y} & -6 & 4l\,n_{ij_x} & 4l\,n_{ij_y} \end{bmatrix} \mathbf{v} \ . \tag{5.3.11}$$

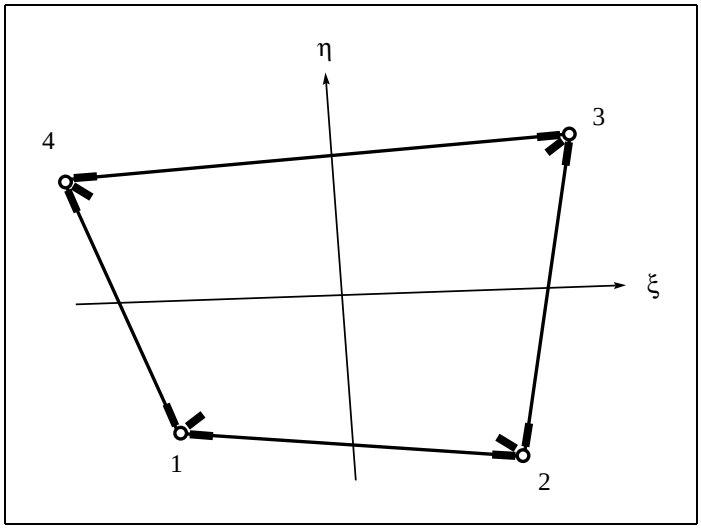

Figure 5.5. Nodal curvature gages for bending.

Nodal natural coordinate curvatures for a quadrilateral.
When one collects all the nodal straingages in a vector $\mathbf{g}$, the strain-gage displacement relationship becomes

$$\mathbf{g} = \mathbf{Q}\mathbf{v} = \mathbf{Q}_F * \mathbf{F}\mathbf{v} \ , \tag{5.3.12}$$

where $*$ denotes entry by entry matrix multiplication, and

$$\begin{aligned} \mathbf{g}^T = [\, &\kappa_{41|1} \quad \kappa_{12|1} \quad \kappa_{13|1} \quad \kappa_{12|2} \quad \kappa_{23|2} \quad \kappa_{24|2} \\ &\kappa_{23|3} \quad \kappa_{34|3} \quad \kappa_{13|3} \quad \kappa_{34|4} \quad \kappa_{41|4} \quad \kappa_{24|4} \,] , \end{aligned} \tag{5.3.13}$$

$$\mathbf{Q}_F = \begin{bmatrix} -6 & 4 & 4 & 0 & 0 & 0 & 0 & 0 & 0 & 6 & 2 & 2 \\ -6 & -4 & -4 & 6 & -2 & -2 & 0 & 0 & 0 & 0 & 0 & 0 \\ -6 & -4 & -4 & 0 & 0 & 0 & 6 & -2 & -2 & 0 & 0 & 0 \\ & & & & & & & & & & & \\ 6 & 2 & 2 & -6 & 4 & 4 & 0 & 0 & 0 & 0 & 0 & 0 \\ 0 & 0 & 0 & -6 & -4 & -4 & 6 & -2 & -2 & 0 & 0 & 0 \\ 0 & 0 & 0 & -6 & -4 & -4 & 0 & 0 & 0 & 6 & -2 & -2 \\ & & & & & & & & & & & \\ 0 & 0 & 0 & 6 & 2 & 2 & -6 & 4 & 4 & 0 & 0 & 0 \\ 0 & 0 & 0 & 0 & 0 & 0 & -6 & -4 & -4 & 6 & -2 & -2 \\ 6 & 2 & 2 & 0 & 0 & 0 & -6 & 4 & 4 & 0 & 0 & 0 \\ & & & & & & & & & & & \\ 0 & 0 & 0 & 0 & 0 & 0 & 6 & 2 & 2 & -6 & 4 & 4 \\ 6 & -2 & -2 & 0 & 0 & 0 & 0 & 0 & 0 & -6 & -4 & -4 \\ 0 & 0 & 0 & 6 & 2 & 2 & 0 & 0 & 0 & -6 & 4 & 4 \end{bmatrix} , \tag{5.3.14}$$

$$\mathbf{F} = \begin{bmatrix} \mathbf{F}_{41} & \mathbf{F}_{41} & \mathbf{F}_{41} & \mathbf{F}_{41} \\ \mathbf{F}_{12} & \mathbf{F}_{12} & \mathbf{F}_{12} & \mathbf{F}_{12} \\ \mathbf{F}_{13} & \mathbf{F}_{13} & \mathbf{F}_{13} & \mathbf{F}_{13} \\ & & & \\ \mathbf{F}_{12} & \mathbf{F}_{12} & \mathbf{F}_{12} & \mathbf{F}_{12} \\ \mathbf{F}_{23} & \mathbf{F}_{23} & \mathbf{F}_{23} & \mathbf{F}_{23} \\ \mathbf{F}_{24} & \mathbf{F}_{24} & \mathbf{F}_{24} & \mathbf{F}_{24} \\ & & & \\ \mathbf{F}_{23} & \mathbf{F}_{23} & \mathbf{F}_{23} & \mathbf{F}_{23} \\ \mathbf{F}_{34} & \mathbf{F}_{34} & \mathbf{F}_{34} & \mathbf{F}_{34} \\ \mathbf{F}_{13} & \mathbf{F}_{13} & \mathbf{F}_{13} & \mathbf{F}_{13} \\ & & & \\ \mathbf{F}_{34} & \mathbf{F}_{34} & \mathbf{F}_{34} & \mathbf{F}_{34} \\ \mathbf{F}_{41} & \mathbf{F}_{41} & \mathbf{F}_{41} & \mathbf{F}_{41} \\ \mathbf{F}_{24} & \mathbf{F}_{24} & \mathbf{F}_{24} & \mathbf{F}_{24} \end{bmatrix} \quad \text{where} \quad \begin{aligned} \mathbf{F}_{12} &= \begin{bmatrix} \frac{1}{l_{12}^2} & \frac{n_{12_x}}{l_{12}} & \frac{n_{12_y}}{l_{12}} \end{bmatrix} \\ \mathbf{F}_{23} &= \begin{bmatrix} \frac{1}{l_{23}^2} & \frac{n_{23_x}}{l_{23}} & \frac{n_{23_y}}{l_{23}} \end{bmatrix} \\ \mathbf{F}_{34} &= \begin{bmatrix} \frac{1}{l_{34}^2} & \frac{n_{34_x}}{l_{34}} & \frac{n_{34_y}}{l_{34}} \end{bmatrix} \\ \mathbf{F}_{41} &= \begin{bmatrix} \frac{1}{l_{41}^2} & \frac{n_{41_x}}{l_{41}} & \frac{n_{41_y}}{l_{41}} \end{bmatrix} \\ \mathbf{F}_{13} &= \begin{bmatrix} \frac{1}{l_{13}^2} & \frac{n_{13_x}}{l_{13}} & \frac{n_{13_y}}{l_{13}} \end{bmatrix} \\ \mathbf{F}_{24} &= \begin{bmatrix} \frac{1}{l_{24}^2} & \frac{n_{24_x}}{l_{24}} & \frac{n_{24_y}}{l_{24}} \end{bmatrix} \end{aligned} . \tag{5.3.15}$$

Cartesian curvatures for a quadrilateral.
The cartesian curvatures $\boldsymbol{\kappa}^T = [\, \kappa_{xx} \quad \kappa_{yy} \quad \kappa_{xy} \,]$ at the nodes can now be obtained as

$$\mathbf{g}_C = \mathbf{Q}_C \mathbf{v} \tag{5.3.16}$$

or

$$\begin{Bmatrix} \boldsymbol{\kappa}_{|1} \\ \boldsymbol{\kappa}_{|2} \\ \boldsymbol{\kappa}_{|3} \\ \boldsymbol{\kappa}_{|4} \end{Bmatrix} = \begin{bmatrix} \mathbf{B}_1 \\ \mathbf{B}_2 \\ \mathbf{B}_3 \\ \mathbf{B}_4 \end{bmatrix} \mathbf{v} = \begin{bmatrix} \mathbf{T}_{\kappa 1} \mathbf{Q}_1 \\ \mathbf{T}_{\kappa 2} \mathbf{Q}_2 \\ \mathbf{T}_{\kappa 3} \mathbf{Q}_3 \\ \mathbf{T}_{\kappa 4} \mathbf{Q}_4 \end{bmatrix} \mathbf{v} \,,$$

where

$$\begin{aligned} \mathbf{T}_{\kappa 1}^{-1} &= \begin{bmatrix} {s_{41}}_x^2 & {s_{41}}_y^2 & s_{41_x} s_{41_y} \\ {s_{12}}_x^2 & {s_{12}}_y^2 & s_{12_x} s_{12_y} \\ {s_{13}}_x^2 & {s_{13}}_y^2 & s_{13_x} s_{13_y} \end{bmatrix} , \\ \mathbf{T}_{\kappa 2}^{-1} &= \begin{bmatrix} {s_{12}}_x^2 & {s_{12}}_y^2 & s_{12_x} s_{12_y} \\ {s_{23}}_x^2 & {s_{23}}_y^2 & s_{23_x} s_{23_y} \\ {s_{24}}_x^2 & {s_{24}}_y^2 & s_{24_x} s_{24_y} \end{bmatrix} , \\ \mathbf{T}_{\kappa 3}^{-1} &= \begin{bmatrix} {s_{23}}_x^2 & {s_{23}}_y^2 & s_{23_x} s_{23_y} \\ {s_{34}}_x^2 & {s_{34}}_y^2 & s_{34_x} s_{34_y} \\ {s_{13}}_x^2 & {s_{13}}_y^2 & s_{13_x} s_{13_y} \end{bmatrix} , \\ \mathbf{T}_{\kappa 4}^{-1} &= \begin{bmatrix} {s_{34}}_x^2 & {s_{34}}_y^2 & s_{34_x} s_{34_y} \\ {s_{41}}_x^2 & {s_{41}}_y^2 & s_{41_x} s_{41_y} \\ {s_{24}}_x^2 & {s_{24}}_y^2 & s_{24_x} s_{24_y} \end{bmatrix} . \end{aligned}$$

The Cartesian curvatures over the element can then be obtained by interpolation of the nodal values as

$$\boldsymbol{\kappa} = \mathbf{B}(\xi, \eta) \mathbf{v} \,, \tag{5.3.17}$$

where

$$\begin{aligned}\mathbf{B}(\xi,\eta) = \quad & (1-\xi)(1-\eta)\mathbf{B}_1 + (1+\xi)(1-\eta)\mathbf{B}_2 \\ & +(1+\xi)(1+\eta)\mathbf{B}_3 + (1-\xi)(1+\eta)\mathbf{B}_4\end{aligned} \ . \tag{5.3.18}$$

Higher order stiffness for the element.
The ANDES higher order stiffness is computed as

$$\mathbf{K}_d = \int_A \mathbf{B}_d^T \mathbf{C} \mathbf{B}_d \, dA \quad \text{where} \quad \mathbf{B}_d = \mathbf{B} - \frac{1}{A}\int_A \mathbf{B} \, dA \ . \tag{5.3.19}$$

5.3.3 The ANS quadrilateral plate bending element.

Clearly one can form an ANS type element by

$$\mathbf{K} = \int_A \mathbf{B}^T \mathbf{C} \mathbf{B} \, dA \tag{5.3.20}$$

i.e. without extracting the mean part of the strain displacement matrix and not including the basic stiffness described in Section 5.3.1.

5.4 The linear non-flat quadrilateral shell element.

The objective of this section is to develop a technique that allows the use of the flat quadrilateral membrane and bending element as parts of a non-flat shell element for linear problems. This is obtained by formulating a linear projector matrix, which for the linear case restores equilibrium at the undeformed element geometry. This can also be obtained by using the nonlinear projector with respect to the initial geometry. In fact the linear and nonlinear projector gives identical results for linear problems. However the linear projector is recommended for linear finite element codes due to its greater simplicity.

The four node shell element is obtained by assembling the membrane element and bending element to the appropriate degrees of freedom. This is sufficient as long as the shell element is strictly flat since both the membrane and bending elements are developed as flat elements. Unfortunately, four node shell elements on a "real" structure quite often end up being warped. To restore or improve the behavior of the warped element one can use a projection technique similar to that developed by Rankin and coworkers [00, 00].

The element stiffness matrix does not have the correct rigid body modes if the element geometry is warped since the element stiffness has been developed using the projected flat positions of the element nodes. This causes two deficiencies of the element stiffness:

1. The element picks up strains and thus forces from a rigid body displacement vector i.e. $\mathbf{f}_r = \mathbf{K}\mathbf{v}_r \neq \mathbf{0}$.

2. The element forces are not in self equilibrium and the force vector will thus pick up energy for a rigid body motion. $\mathbf{v}_r^T\mathbf{f} = \mathbf{v}_r^T\mathbf{K}\mathbf{v} \neq \mathbf{0}$.

These two statements are equivalent for a symmetric element stiffness matrix. If an element stiffness has columns that are in self equilibrium the element has the correct rigid body modes and vice versa.

The foregoing deficiencies lead to the investigation of the element internal energy

$$\begin{aligned}\Phi &= \frac{1}{2}\mathbf{v}^T\mathbf{K}\mathbf{v} = \frac{1}{2}(\mathbf{v}_r^T + \mathbf{v}_d^T)\mathbf{K}(\mathbf{v}_r + \mathbf{v}_d) \\ &= \frac{1}{2}(\mathbf{v}_d^T\mathbf{K}\mathbf{v}_d + \mathbf{v}_d^T\mathbf{K}\mathbf{v}_r + \mathbf{v}_r^T\mathbf{K}\mathbf{v}_d + \mathbf{v}_r^T\mathbf{K}\mathbf{v}_r).\end{aligned} \tag{5.4.1}$$

If the element fails the equilibrium and rigid-body conditions;

$$\mathbf{v}_r^T\mathbf{K}\mathbf{v}_r \neq 0\ , \quad \mathbf{v}_r^T\mathbf{K}\mathbf{v}_d \neq 0 \quad \text{and} \quad \mathbf{v}_d^T\mathbf{K}\mathbf{v}_r \neq 0\ . \tag{5.4.2}$$

To extract the deformational energy, the total displacements are split into deformational and rigid body motions, the latter being spanned by the matrix $\mathbf{R}$:

$$\mathbf{v} = \mathbf{v}_d + \mathbf{v}_r = \mathbf{v}_d + \mathbf{R}\mathbf{a}. \tag{5.4.3}$$

By requiring that the deformational displacement vector be orthogonal to the rigid body modes one must have $\mathbf{R}^T\mathbf{v}_d = \mathbf{0}$. On pre-multiplying the equation above with $\mathbf{R}^T$ the rigid body amplitudes can be solved for:

$$\mathbf{R}^T\mathbf{v} = \mathbf{R}^T\mathbf{R}\mathbf{a} \quad \Rightarrow \quad \mathbf{a} = (\,\mathbf{R}^T\mathbf{R}\,)^{-1}\mathbf{R}\mathbf{v}\ , \tag{5.4.4}$$

from which the deformational displacement vector can be extracted as

$$\mathbf{v}_d = \mathbf{v} - \mathbf{v}_r = (\,\mathbf{I} - \mathbf{R}\,(\,\mathbf{R}^T\mathbf{R}\,)^{-1}\mathbf{R}\,)\,\mathbf{v} = \mathbf{P}_d\mathbf{v}. \tag{5.4.5}$$

If $\mathbf{R}$ is orthonormal the foregoing expression simplifies to

$$\mathbf{P}_d = \mathbf{I} - \mathbf{R}\mathbf{R}^T. \tag{5.4.6}$$

Applying this projection to gain invariance of the internal energy with respect to rigid body motion $\Phi(\mathbf{v}) = \Phi(\mathbf{v}_d)$ yields

$$\Phi(\mathbf{v}_d) = \frac{1}{2}\mathbf{v}_d^T\mathbf{K}\mathbf{v}_d = \frac{1}{2}\mathbf{v}^T\mathbf{P}_d^T\mathbf{K}\mathbf{P}_d\mathbf{v} = \frac{1}{2}\mathbf{v}^T\mathbf{K}_d\mathbf{v}\ . \tag{5.4.7}$$

5.4.1 Linear projector matrix for a general quad.

In order to express the rigid body modes one defines the vector $\mathbf{r}_i$ from the element centroid to node i as

$$\tilde{\mathbf{r}}_i = \mathbf{r}_i - \bar{\mathbf{r}} \ , \quad \text{where} \quad \mathbf{r}_i = \left\{ \begin{array}{c} x_i \\ y_i \\ z_i \end{array} \right\} \quad \text{and} \quad \bar{\mathbf{r}} = \frac{1}{4} \sum_{i=1}^{4} \mathbf{r}_i \ . \tag{5.4.8}$$

By ordering the element degrees of freedom as

$$\mathbf{v} = \left\{ \begin{array}{c} \mathbf{v}_1 \\ \mathbf{v}_2 \\ \mathbf{v}_3 \\ \mathbf{v}_4 \end{array} \right\} \qquad \text{where} \qquad \mathbf{v}_i = \left\{ \begin{array}{c} v_{xi} \\ v_{yi} \\ v_{zi} \\ \theta_{xi} \\ \theta_{yi} \\ \theta_{zi} \end{array} \right\} \tag{5.4.9}$$

the rigid body modes can be expressed as

$$\mathbf{R} = \begin{bmatrix} \mathbf{R}_1 \\ \mathbf{R}_2 \\ \mathbf{R}_3 \\ \mathbf{R}_4 \end{bmatrix}, \qquad \mathbf{R}_i = \begin{bmatrix} \mathbf{I} & -\text{Spin}(\tilde{\mathbf{r}}_i) \\ \mathbf{0} & \mathbf{I} \end{bmatrix} = \begin{bmatrix} 1 & 0 & 0 & 0 & \tilde{z}_i & -\tilde{y}_i \\ 0 & 1 & 0 & -\tilde{z}_i & 0 & \tilde{x}_i \\ 0 & 0 & 1 & \tilde{y}_i & -\tilde{x}_i & 0 \\ 0 & 0 & 0 & 1 & 0 & 0 \\ 0 & 0 & 0 & 0 & 1 & 0 \\ 0 & 0 & 0 & 0 & 0 & 1 \end{bmatrix} . \tag{5.4.10}$$

The projector matrix becomes

$$\mathbf{P}_d = \mathbf{I} - \mathbf{R}(\mathbf{R}^T\mathbf{R})^{-1}\mathbf{R}^T \ , \tag{5.4.11}$$

where

$$\mathbf{R}^T\mathbf{R} = \begin{bmatrix} 4\mathbf{I} & \mathbf{0} \\ \mathbf{0} & \mathbf{S} \end{bmatrix} \quad \text{with} \quad \mathbf{S} = 4\mathbf{I} - \sum_{i=1}^{4} \text{Spin}(\tilde{\mathbf{r}}_i)\text{Spin}(\tilde{\mathbf{r}}_i) \ .$$

This simplifies the computation of the projector matrix because only the lowest 3×3 submatrix of $\mathbf{R}^T\mathbf{R}$ is non-diagonal, and $(\mathbf{R}^T\mathbf{R})^{-1}$ can be efficiently formed.

5.5 Nonlinear extensions for quadrilateral shell element.

The nonlinear extensions for an element consists of defining a procedure that aligns the shadow element C_{0n} as close as possible to the deformed element C_n. This defines the element deformational displacement vector $\mathbf{v}_d$.

One also needs to form the rotational gradient of the shadow element with respect to the visible degrees of freedom of the deformed element, as stated in equation (0.0.0). In the local coordinate system this relation is

$$\delta\tilde{\boldsymbol{\omega}}_r = \frac{\partial\tilde{\boldsymbol{\omega}}_r}{\partial\tilde{v}_i}\delta v_i = \tilde{\mathbf{G}}\,\delta\tilde{\mathbf{v}}\ . \tag{5.5.1}$$

The local coordinate relationship is sought since this is is needed in forming the geometric stiffness of the element as expressed in equation (0.0.0) .

The rotation of the shadow element is most easily obtained from the rotation of the shared or common local frame for the C_{0n} and C_n configurations. This orthogonal element coordinate frame with unit axis vectors $\mathbf{e}_1$, $\mathbf{e}_2$ and $\mathbf{e}_3$ is rigidly attached to the shadow element C_{0n}, since this element only moves as a rigid body, and elastically attached to the deformed and elastic element C_n. This local coordinate system for a quadrilateral element can be defined in various ways. Most researchers select the element z-axis unit vector as the cross product of the diagonals vectors $\mathbf{d}_{13}$ and $\mathbf{d}_{24}$

$$\mathbf{e}_3 = \frac{\mathbf{d}_{13}\times\mathbf{d}_{24}}{A_p} \quad \text{where} \quad A_p = \sqrt{(\mathbf{d}_{13}\times\mathbf{d}_{24})^T(\mathbf{d}_{13}\times\mathbf{d}_{24})} \tag{5.5.2}$$

This defines A_p as the area of the element projection on the local $x-y$ plane.

The positioning of the x and y axis unit vectors $\mathbf{e}_1$ and $\mathbf{e}_2$ differs among researchers. Rankin and Brogan [00] chooses $\mathbf{e}_2$ to coincide with the projection of the side edge 24 on the plane normal to $\mathbf{e}_3$. This effectively lets only one of the side edges determine the rigid rotation of the element about the local z axis. The origin of the element coordinate system is chosen to coincide with node 1. When this procedure is performed for both the C_0 and C_n element configurations the net result is that the shadow element C_{0n} will be positioned relative to C_n so that nodes 1 coincide and the projections of side edge 24 on the (x, y) plane coincide. A consequence of this choice is that the element deformational displacement vector $\mathbf{v}_d$, which is the difference between the coordinate between the C_n and C_{0n} coordinates, is not invariant with respect to the element node numbering.

Bergan and Nygård [00] choose vector $\mathbf{e}_1$ and $\mathbf{e}_2$ to coincide with the directions of side edge 12 and 14 for a rectangle that is positioned relative to the quadrilateral element so that the sum of the angles between the side edges of the quadrilateral and rectangle is zero. The origin of the coordinate system

is chosen at node 1. By applying this to both the C_0 and C_n configurations the shadow element C_{0n} is positioned relative to the deformed element C_n so that the element centroids coincide and so that the sum of the square of the angles between the side edges of C_{0n} and C_n is minimized. This represents a least square fit with respect to the side edge angular errors. This procedure gives a element deformational displacement vector $\mathbf{v}_d$ which produces an internal force vector $\mathbf{f}_e = \mathbf{K}_e\mathbf{v}_d$ that is invariant with respect to the node numbering of the element, provided that the element stiffness matrix $\mathbf{K}_e$ satisfies the correct rigid body translations.

5.5.1 Aligning side 12 of C_{0n} and C_n.

The element frame is positioned at the element centroid. This change from Rankin's positioning at node 1 has been done in order to satisfy the orthogonality condition for $\mathbf{P}_T\mathbf{P}_R = \mathbf{0}$ as expressed in equation (0.0.0) . Rankin's formulation did not contain $\mathbf{P}_T$ so this requirement was ignored.

By expressing the nodal coordinates of the element in the local coordinate system equation (5.5.2) gives

$$\tilde{\mathbf{e}}_3 = \begin{Bmatrix} \tilde{e}_{3x} \\ \tilde{e}_{3y} \\ \tilde{e}_{3z} \end{Bmatrix} = \frac{1}{A_p} \begin{Bmatrix} \tilde{y}_{31}\tilde{z}_{42} - \tilde{y}_{42}\tilde{z}_{31} \\ -\tilde{x}_{31}\tilde{z}_{42} + \tilde{x}_{42}\tilde{z}_{31} \\ \tilde{x}_{31}\tilde{y}_{42} - \tilde{x}_{42}\tilde{y}_{31} \end{Bmatrix}, \tag{5.5.3}$$

where

$$A_p = \sqrt{(\tilde{y}_{31}\tilde{z}_{42} - \tilde{y}_{42}\tilde{z}_{31})^2 + (-\tilde{x}_{31}\tilde{z}_{42} + \tilde{x}_{42}\tilde{z}_{31})^2 + (\tilde{x}_{31}\tilde{y}_{42} - \tilde{x}_{42}\tilde{y}_{31})^2}\ . \tag{5.5.4}$$

These expressions simplify, but the full expressions has to be kept in order to obtain the correct variation with respect to the nodal coordinates. The $\tilde{\omega}_x$ and $\tilde{\omega}_y$ variation can now be obtained from the variation of e_{3y} and e_{3x} respectively

$$\begin{aligned} \delta\tilde{\omega}_x &= -(\frac{\partial\tilde{e}_{3y}}{\partial\tilde{x}_i}\delta\tilde{x}_i + \frac{\partial\tilde{e}_{3y}}{\partial\tilde{y}_i}\delta\tilde{y}_i + \frac{\partial\tilde{e}_{3y}}{\partial\tilde{z}_i}\delta\tilde{z}_i)\ , \\ \delta\tilde{\omega}_y &= \ \ (\frac{\partial\tilde{e}_{3x}}{\partial\tilde{x}_i}\delta\tilde{x}_i + \frac{\partial\tilde{e}_{3x}}{\partial\tilde{y}_i}\delta\tilde{y}_i + \frac{\partial\tilde{e}_{3x}}{\partial\tilde{z}_i}\delta\tilde{z}_i)\ . \end{aligned} \tag{5.5.5}$$

The variation of $\tilde{\omega}_x$ and $\tilde{\omega}_y$ with respect to the in-plane coordinate components of the nodes $\tilde{x}_i$ and $\tilde{y}_i$ is zero since

$$\frac{\partial\tilde{e}_{3x}}{\partial\tilde{x}_i} = \frac{\partial\tilde{e}_{3x}}{\partial\tilde{y}_i} = \frac{\partial\tilde{e}_{3y}}{\partial\tilde{x}_i} = \frac{\partial\tilde{e}_{3y}}{\partial\tilde{y}_i} = 0\ . \tag{5.5.6}$$

This gives the variation of the in-plane rotations $\tilde{\omega}_x$ and $\tilde{\omega}_y$ as function of the out of plane displacements only:

$$\begin{aligned} \delta\tilde{\omega}_x &= -\frac{\partial \tilde{e}_{3x}}{\partial \tilde{z}_i}\delta\tilde{z}_i = \sum_{i=1}^{4} \frac{\tilde{x}_{lj}}{A_p}\delta\tilde{z}_i \ , \\ \delta\tilde{\omega}_y &= \ \ \frac{\partial \tilde{e}_{3y}}{\partial \tilde{z}_i}\delta\tilde{z}_i = \sum_{i=1}^{4} \frac{\tilde{y}_{lj}}{A_p}\delta\tilde{z}_i \ , \end{aligned} \qquad \text{with} \quad A_p = \tilde{x}_{31}\tilde{y}_{42} - \tilde{x}_{42}\tilde{y}_{31} \ , \tag{5.5.7}$$

where the nodal indices (i, j, k, l) takes cyclic permutations of $(1, 2, 3, 4)$.

The $\mathbf{e}_1$ vector is chosen to lie along the projection of side 12 in the x-y plane. This gives the y axis unit vector as

$$\mathbf{e}_2 = \frac{\mathbf{e}_3 \times \mathbf{r}_{12}}{l_{12}} \ , \tag{5.5.8}$$

where l_{12} is the projected length of side 12 in the x-y plane. By expressing $\mathbf{e}_2$ in the local coordinate system the variation of $\tilde{\omega}_z$ can be obtained as

$$\delta\tilde{\omega}_z = -(\frac{\partial \tilde{e}_{2x}}{\partial \tilde{x}_i}\delta\tilde{x}_i + \frac{\partial \tilde{e}_{2x}}{\partial \tilde{y}_i}\delta\tilde{y}_i + \frac{\partial \tilde{e}_{2x}}{\partial \tilde{z}_i}\delta\tilde{z}_i) \ . \tag{5.5.9}$$

Carrying out the derivations gives

$$\delta\tilde{\omega}_z = \frac{1}{l_{12}}(\delta\tilde{y}_1 + \delta\tilde{y}_2) - \sum_{i=1}^{4} \frac{\tilde{x}_{lj}\, z_{21}}{A_p}\delta\tilde{z}_i \ , \tag{5.5.10}$$

where A_p is defined in equation (5.5.7).

The rotation gradient matrix in equation (5.5.1) can now be expressed as

$$\tilde{\mathbf{G}} = [\, \tilde{\mathbf{G}}_1 \quad \tilde{\mathbf{G}}_2 \quad \tilde{\mathbf{G}}_3 \,] = \begin{bmatrix} \tilde{\mathbf{G}}_{\omega_x} \\ \tilde{\mathbf{G}}_{\omega_y} \\ \tilde{\mathbf{G}}_{\omega_z} \end{bmatrix} \tag{5.5.11}$$

where

$$\begin{aligned} \tilde{\mathbf{G}}_1 &= \frac{1}{A_p}\begin{bmatrix} 0 & 0 & x_{42} & 0 & 0 & 0 \\ 0 & 0 & y_{42} & 0 & 0 & 0 \\ 0 & -\frac{A_p}{l_{12}} & x_{42}z_{21} & 0 & 0 & 0 \end{bmatrix}, \\ \tilde{\mathbf{G}}_2 &= \frac{1}{A_p}\begin{bmatrix} 0 & 0 & x_{13} & 0 & 0 & 0 \\ 0 & 0 & y_{13} & 0 & 0 & 0 \\ 0 & \frac{A_p}{l_{12}} & x_{13}z_{21} & 0 & 0 & 0 \end{bmatrix}, \\ \tilde{\mathbf{G}}_3 &= \frac{1}{A_p}\begin{bmatrix} 0 & 0 & x_{24} & 0 & 0 & 0 \\ 0 & 0 & y_{24} & 0 & 0 & 0 \\ 0 & 0 & x_{24}z_{21} & 0 & 0 & 0 \end{bmatrix}, \\ \tilde{\mathbf{G}}_4 &= \frac{1}{A_p}\begin{bmatrix} 0 & 0 & x_{31} & 0 & 0 & 0 \\ 0 & 0 & y_{31} & 0 & 0 & 0 \\ 0 & 0 & x_{42}z_{31} & 0 & 0 & 0 \end{bmatrix}. \end{aligned} \tag{5.5.12}$$

The rotation gradient matrix as expressed here can be split as $\tilde{\mathbf{G}} = \tilde{\mathbf{X}}\mathbf{A}$ where $\tilde{\mathbf{X}}$ contains all the coordinate dependencies and $\mathbf{A}$ is constant matrix. This is possible since none of the vector components of $\delta\tilde{\boldsymbol{\omega}}$ is a function of more than three distinct coordinate expressions. This $\tilde{\mathbf{G}}$ thus satisfies the consistency requirement set forth in equation (0.0.0).

5.5.2 Least square fit of side edge angular errors.

The orientation of $\mathbf{e}_3$ is the same as with Rankin's procedure, which gives identical expressions for the rotations $\tilde{\omega}_x$ and $\tilde{\omega}_y$. The positioning procedure of Bergan and Nygårds [00] positioning procedure can be viewed as a least square fit of the side edge angular errors between the C_{0n} and C_n configurations. This gives different expressions for the variation of the angle $\tilde{\omega}_z$ with respect to the visible degrees of freedom. The nodal submatrices $\tilde{\mathbf{G}}_i$ of $\tilde{\mathbf{G}}$ can then be defined as

$$\mathbf{G}_i = \frac{1}{A_p}\begin{bmatrix} 0 & 0 & x_{lj} & \\ 0 & 0 & y_{lj} & \mathbf{0} \\ \frac{A_p}{4}(\frac{n_{ij\,x}}{l_{ij}} - \frac{n_{ki\,x}}{l_{ki}}) & \frac{A_p}{4}(\frac{n_{ij\,y}}{l_{ij}} - \frac{n_{ki\,y}}{l_{ki}}) & (x_{lj}f_x + y_{lj}f_y) & \end{bmatrix}, \quad (5.5.13)$$

where

$$\begin{aligned} f_x &= \frac{1}{4}(\frac{z_{21}x_{21}}{l_{21}} + \frac{z_{32}x_{32}}{l_{32}} + \frac{z_{43}x_{43}}{l_{43}} + \frac{z_{14}x_{14}}{l_{14}}) \,, \\ f_y &= \frac{1}{4}(\frac{z_{21}y_{21}}{l_{21}} + \frac{z_{32}y_{32}}{l_{32}} + \frac{z_{43}y_{43}}{l_{43}} + \frac{z_{14}y_{14}}{l_{14}}) \,, \end{aligned} \quad (5.5.14)$$

and $\tilde{\mathbf{n}}_{ij}$ and l_{ij} is the outward normal and length of side edge ij respectively:

$$\mathbf{n}_{ij} = \frac{1}{l_{ij}}\begin{Bmatrix} y_{ji} \\ -x_{ji} \\ 0 \end{Bmatrix} \quad \text{and} \quad l_{ij} = \sqrt{x_{ij}^2 + y_{ij}^2} \,. \quad (5.5.15)$$

The nodal indices (i, j, k, l) undergo cyclic permutations of $(1, 2, 3, 4)$.

The $\tilde{\mathbf{G}}$ derived above can not be expressed as $\tilde{\mathbf{G}} = \tilde{\mathbf{X}}\mathbf{A}$ where the 3×3 matrix $\tilde{\mathbf{X}}$ contains all the coordinate dependencies of $\tilde{\mathbf{G}}$, since the expressions for $\tilde{\omega}_z$ contains more than three distinct coordinate expressions. This will give a loss in convergence rate if the deformed configuration C_n and shadow configuration C_{0n} are far apart since the present tangent stiffness expressions have omitted terms containing the unbalanced element forces. See Section 0.0.0.